CO rate and BHMG: A Writeup

Vaishnav V. Rao, Harshda Saxena

September 7, 2022

Contents

1 Astrophysical nuclear reaction basics Descouvemont (2020)

In the low energy regime, the scattering between charged particles is essentially governed by the Coulomb interaction. The solutions to the Schrodinger equation with a simple Coulombic interaction are the regular and irregular Coulomb functions. From this, the penetration factor P_L can be obtained. The penetration factor can be approximately interpreted as the probability to cross the Coulomb barrier, and therefore strongly depends on energy (strictly speaking, however, P_L is not a probability since it may be larger than unity). Below the Coulomb barrier, it essentially depends on energy as

$$P_L(E, a) \sim \exp(-2\pi\eta)$$

where $\eta = 0.158 Z_1 Z_2 \sqrt{\mu/E}$ (E in meV) is the Sommerfeld parameter.

The fast energy dependence is common to all low-energy cross sections. For this reason, nuclear astrophysicists use the S factor

$$S(E) = \sigma(E) E \exp(2\pi\eta)$$

which presents a smooth energy dependence for non-resonant reactions. It contains the nuclear information on the reaction. Since the energy-dependent variation of the astrophysical S-factor is much slower than the energy-dependent change of the cross-section, it is much more convenient to extrapolate the astrophysical S-factor to lower energies where experimental cross-section measurement is not possible. Employing this $S(E)$ factor in calculating the average crosssection, The integrand is a product of the probability of a charged particle pair having energy E and the tunneling probability for that energy. The energy dependent terms of $S(E)$ winds up making the reaction rate integral have several temperature dependent factors, which is how the databases work.

For photodisintegration, given that photons follow a Planck distribution, the ratio of the back and forward rate crossections become :

$$\frac{\langle \sigma\nu \rangle_{3\gamma}}{\langle \sigma\nu \rangle_{12}} = \left(\frac{\mu_{12} c^2}{k_B T} \right)^{3/2} exp\left(- \frac{Q_{12}}{k_B T} \right)$$

Reaction channels: In nuclear reaction, each possible combination of nuclei is called a partition. Each partition further distinguished by state of excitation of each nucleus and each such pair of states is known as a reaction channel.

1.1 R-matrix theory from first principles

The phenomenological R matrix offers an efficient way for accurately parametrizing low-energy cross sections with a small number of parameters. The basic idea is to divide the space in two regions: the internal region where the nuclear force is important and has complicated many body interactions, and the external region with 2 clusters, where the interaction between the nuclei is governed by the Coulomb force only. They are separated by a boundary called the channel radius. The R matrix is just calculated in the interior region, which has a central potential $V(r)$. Inside, the Hamiltonian is written as $(H_l - E)u_l = 0$, where $H_l = -\frac{h^2}{2\mu}(\frac{d^2}{dr^2} - \frac{l(l+1)}{r^2})$. Outside, the wavefunction is described as

$$u_l^{ext}(r) = I_l(kr) - U_l O_l(kr)$$

, where I, O are the incoming and outgoing wavefunctions, composed of the regular and irregular Coulomb functions (solutions to the Coulombic potentials) and U_l is the scattering matrix $U_l = e^{2i\delta_l}$. Internally, the wave function is expanded over some basis as

$$u_l^{int}(r) = \sum c_j \phi_j(r)$$

Note that the Hamiltonian H_l is not Hermitian over the internal region, with the Wronskian appearing there, the problem of which is solved by introducing a surface operator, $\mathcal{L} = \frac{h^2}{2\mu}\delta(r-a)\frac{d}{dr}$, which thus makes $H_l+\mathcal{L}$ Hermitian. The Schrodinger equation in the internal region is approximated by the inhomogeneous Bloch-Schrodinger equation

$$(H_l + \mathcal{L} - E)u_l^{int} = \mathcal{L}u_l^{expt}$$

This solution is clearly equivalent to $(H_l - E)u_l^{int} = 0$ and $u_l'^{int}(a) = u_l'^{ext}(a)$. Including the continutity condition, this is the same way we solve the Schrodinger equation.

The R matrix at energy E is defined as

$$u_l(a) = R_l(E)au_l'(a)$$

, and the R matrix can be calculated from properties of the Hamiltonian in the internal region. Expanding in terms of the basis, this gives the R-matrix as

$$R_l(E) = \frac{h^2}{2\mu a}\sum \phi_i(a)(C^{-1})_{ij}\phi_j(a)$$

, where $C_{ij} = \langle\phi_i|T_l + V + \mathcal{L} - E|\phi_j\rangle$, and this can help us define the wavefunction in the internal region. It also helps extract the phase shift of the lth partial wave as $tan\delta_l = -\frac{F_l(ka)-kaR_l(E)F_l'(ka)}{G_l(ka)-kaR_l(E)G_l'(ka)}$, and $\phi_l = -arctan(F_l(ka)/G_l(ka))$ is the hard-sphere phase shift.

If we consider E_{nl}, v_{nl} as the eigenvalues and eigenvectors for C(0), the R matrix can be expanded as $R_l(E) = \sum \frac{\gamma_{nl}^2}{E_{nl}-E}$ with the numberator being the reduced widths, which are expressed in terms of v_{nl}, ϕ_i. We can further describe the penetration and shift factors (S_l).

Near a resonance, for the phase shifts we get the Breit-Wigner form as

$$\delta_l = \phi_l + arctan\frac{\Gamma(E)/2}{E_R - E}$$

with the resonance energy $E_R = E_{nl} - \gamma_{nl}^2 S_l E(R)$ and the formal width $\Gamma(E) = 2\gamma_{nl}^2 P_l(E)$. Here S and P are the shift and penetration factors. For elastic scattering data sets are fitted simultaneously by using E_R and Γ_R of the resonant partial waves as adjustable parameters in the single-pole approximation.

1.2 R-matrix theory essentials

Each channel is labeled by the α describing the pair of nuclei, and the coupled spin and relative angular momentum of the pair.

Channel surface functions are utilized to describe total angular momentum J and component M, and can be used to project a total wave function into a well-defined angular momentum state on a particular channel surface, called $|ScJM\rangle$. In the internal region, we take the basis vectors $|\lambda JM\rangle$

to be the solutions to the nuclear Hamiltonian with energy eigenvalues E_λ. The real M independent reduced-width amplitudes are given by $\gamma_{\lambda cJ} = \langle SCJM|\lambda JM\rangle$. Outside, the wavefunctions are defined using incoming and outgoing Coloumb functions deBoer et al. (2017).

By expanding an arbitrary wavefuntion in terms on the inner basis, we can see that

$$\langle c|\Psi\rangle = \sum_{c'} R_{cc'}\langle c'|\frac{\partial}{\partial r_{\alpha'}}r_{\alpha'} - B_{c'}|\Psi\rangle$$

Where $R_{cc'}$ are the elements of the R matrix. One may expect the Breit-Wigner formula to be a particularly good approximation to R-matrix theory in the case of an isolated narrow resonance, such that the importance of other resonances and any nonlinear energy dependencies are negligible Descouvemont (2020).

In the phenomenological variant of the R-matrix method, the physics of the internal region is determined by a number N of poles, which are characterized by their energies E_λ and reduced widths $\gamma_{\lambda c}$. In a multichannel problem, the R-matrix at energy E is defined as

$$R_{c'c} = \sum_{\lambda} \frac{\gamma_{\lambda c'}\gamma_{\lambda c}}{E_\lambda - E}$$

which must be determined for each partial wave with total angular momentum J and component M (here, c describes the channel). Essentially, R defines the logarithmic derivative of the radial wave function at the channel surface(s) as a function of energy.

The general wave function $|\Psi\rangle$ may be expanded in the external region (i.e., outside the channel radii) via

$$|\Psi\rangle_{ext} = \sum_{cJM} z_{cJM}\big[|IcJM\rangle - \sum_{c'} U^J_{cc'}|Oc'JM\rangle\big]$$

where the expansion coefficients z_{cJM} specify the incoming flux, which can only be non zero for open channels and $U_{cc'}$ are elements of the scattering matrix $\mathbf{U}$ (also called the collision matrix). Here, $|IcJM\rangle$ and $|OcJM\rangle$ are the incoming and outgoing Coulomb functions respectively. Demanding continuity between internal and external regions, $\mathbf{U}$ can be related to $\mathbf{R}$ through

$$\mathbf{U} = \omega\{\mathbf{1} + 2i\mathbf{P}^{1/2}[\mathbf{1} - \mathbf{R}(\mathbf{L} - \mathbf{B})]^{-1}\mathbf{R}\mathbf{P}^{1/2}\}\mathbf{\Omega}$$

where $\mathbf{\Omega}, \mathbf{P}, \mathbf{L}$ and $\mathbf{B}$ are purely diagonal with elements Ω_c, P_c, L_c and B_c respectively.

For the calculation of observables, we define the transition matrix to be

$$T_{cc'} = e^{2i\omega_c}\delta_{cc'} - U_{cc'}$$

The angle-integrated cross section can then be calculated via

$$\sigma_{\alpha\alpha'} = \frac{\pi}{k^2_\alpha}\sum_{Jll'ss'} g_J|T_{cc'}|^2$$

where the case of elastic scattering of charged particles is excluded. The statistical factor is given by

$$g_J = \frac{2J+1}{(2J_{\alpha1}+1)(2J_{\alpha2}+1)}$$

where $J_{\alpha1}$ and $J_{\alpha2}$ are the individual particle spins for the pair α.

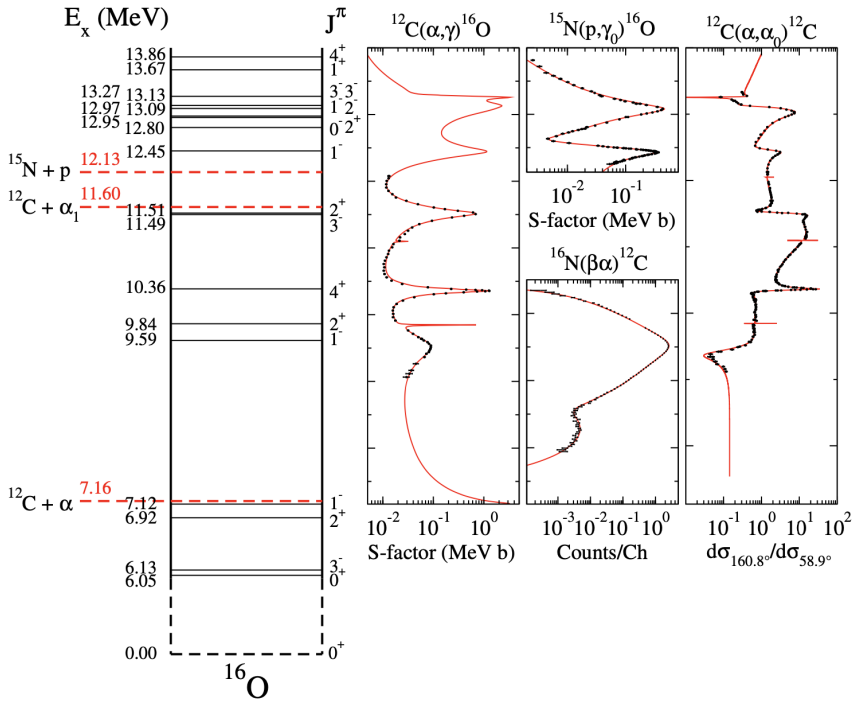

Figure 1: Level diagram of the ^{16}O compound nucleus. 7.16 Mev is the excess energy released when 16O is formed from 12C+α.

1.3 The R-matrix analysis for CO reaction

In implementing the R-matrix formalism, the channel radii still need to be specified. In principle a different radius can be chosen for each channel, but it is common practice to only choose different radii for different partitions. One of the main reasons that the CO cross section has such large uncertainties in the extrapolation is that there are different possible fit solutions, corresponding to the different relative interference patterns of the different resonances, depending on different assumptions and interpretations of the data. **?** found the important conclusions brought about by a thorough review of the data and the R -matrix fits are as follows:

- The $^{12}C(\alpha,\gamma)^{16}O$ E2 ground state transition cross section data show large deviations between one another
- Background pole contributions are negligible for the capture data for all transitions
- For the ground state data, the low- energy measurements yielding larger cross sections are more likely to be affected by unreported sys- tematic uncertainties

These analyses are usually performed using a phenomenological R-matrix analysis but are often complicated by the presence of broad resonance contributions and the need for background contributions. The best fit obtained by deBoer et al. (2017) was not the fit with the lowest overall χ^2, nor was it the fit that allowed all possible parameters to vary freely, but it is believed to be the most

physically reasonable one. In principle a χ^2 minimization should lead to the best solution, but this assumes that all of the uncertainties have been correctly quantified in the data, and this is certainly not the case. χ^2 is defined as follows:

$$\chi^2 = \sum_i \left(\sum_j R_{ij}^2 + \frac{(n_i - 1)^2}{\sigma_{syst,i}^2} \right)$$

where

$$R_{ij} = \frac{f(x_{i,j}) - n_i y_{i,j}}{n_i \sigma_{i,j}}$$

where n_i is the normalization factor of an individual data set, $f(x_{i,j})$ is the value of the cross section from the R-matrix fit, $y_{i,j}$ is the experimental cross section of a given data point, $\sigma_{i,j}$ is the statistical uncertainty of the data point, and $\sigma_{syst,i}^2$ is the overall fractional systematic uncertainty of the data set.

Finally, The stellar reaction rate for the CO reaction was calculated as a sum of nonresonant, or broad resonant, S-factor contributions that were determined through the R-matrix analysis by numerical integration of the average crossection equation, and narrow resonance contributions that were calculated through a Breit-Wigner approximation.

1.4 Ground state transitions

The largest contribution to the $^{12}\mathrm{C}(\alpha,\gamma)^{16}\mathrm{O}$ cross section at low energy (E_{cm} ~300 keV) is the ground state transition. The E1 and E2 multipolarities dominate the low-energy cross section in nearly equal amplitudes. The E1 cross section was also isolated experimentally by measuring at 90deg where σ_{E2} and the interference terms were thought to be zero. Complications arose when it was found that σ_{E2} was also significant. From an experimental standpoint, the immediate difficulty was that there is no angle where σ_{E1} is zero and σ_{E2} is not, therefore σ_{E2} must be deduced indirectly. The traditional technique is to measure the differential cross section at several angles, spanning a wide angular range, and then perform a fit to a theory motivated function representing the angular distribution. If only E1 and E2 multipolarities contribute to the cross section, the differential cross section can be written as

$$4\pi \left(\frac{d\sigma}{d\Omega}\right)(E,\theta_\gamma) = \sigma_{E_1}(E)[1 - Q_2 P_2(\cos\theta_\gamma)] + \sigma_{E_2}(E)\left[1 + \frac{5}{7}Q_2 P_2(\cos\theta_\gamma) - \frac{12}{7}Q_4 P_4(\cos\theta_\gamma)\right] + 6\cos\phi(E)\sqrt{\frac{\sigma_{E_1}(E)\sigma_{E_2}}{5}}$$

where $P_n(\cos\theta_\gamma)$ are the Legendre polynomials, Q_n are the geometric correction factors, and ϕ is the difference in phase between the E1 and E2 transition matrix elements. The phase difference can be written as

$$\cos\phi = \cos[\delta_{\alpha_1} - \delta_{\alpha_2} - \tan^{-1}(\eta/2)]$$

where $\delta_{\alpha 1,2}$ are the angular momentum $l = 1$ and 2α scattering phase shifts and η is the Sommerfeld parameter. This simply illustrates the connection between the scattering cross section, from which the phase shifts can be extracted, and the capture cross section. Since the scattering cross section is large, the phase shifts can be easily and accurately measured and used to constrain $\cos\phi$ up to an overall sign. If σ_{E1} is then determined from measurements at 90deg, then σ_{E2} is essentially the only undetermined quantity. In principle this provides a straightforward way of obtaining σ_{E2} but there are complications. The main issue is that σ_{E1} is much larger than σ_{E2} over much of the experimentally accessed low-energy range because the cross section is dominated by the broad resonance

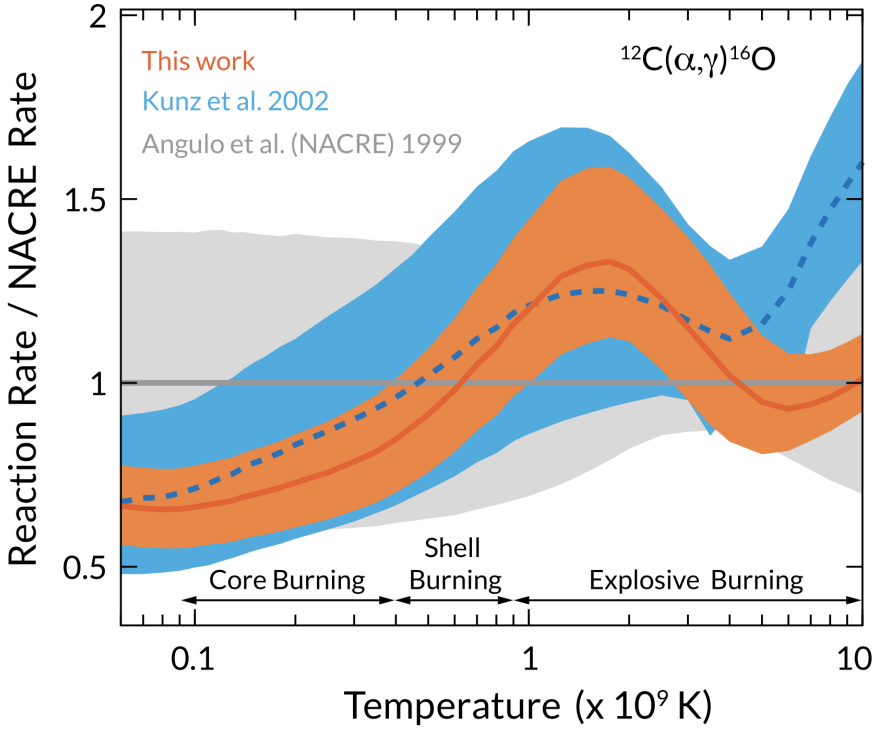

Figure 2: Comparison of the reaction rate and uncertainty calculated in the work of deBoer et al. (2017) (orange band, solid central line) and that from Kunz et al. (2002) (blue band, dashed central line) normalized to the adopted value from Angulo et al. (1999) (NACRE compilation) (gray band, solid central line). The deviations at higher temperature are the result of the different narrow resonance and cascade transitions that were considered in the different works.

corresponding to the 1^- level at E_x =9.59 MeV. The fact that the interference term is proportional to $\sqrt{\sigma_{E1}\sigma_{E2}}$ increases the sensitivity to the small E2 component, but in practice this approach has yielded a large scatter in the σ_{E2} data.

For the E1 data, only decays from 1 levels can contribute because the spins of the entrance channel particles and the final state are all zero. The different levels that are considered are the subthreshold state at E_x = 7.12 MeV and the unbound states at E_x = 9.59, 12.45, and 13.10 MeV. The situation is similar for the E2 data where only 2^+ states can contribute. The states that are considered explicitly are the subthreshold at E_x = 6.92 MeV and two unbound ones at E_x = 11.51 and 12.96 MeV. The narrow state at E_x = 9.84 MeV is also included but its energy and partial widths are all fixed to the values in the literature.

Our understanding: The R-matrix analysis is used to determine the cross sections/S-factors for individual nuclear reaction channels that take the compound $\alpha + ^{12}C$ nucleus to the 1^- and 2+ states of the excited oxygen nucleus O^*. All the 1^- states decay to the ground state (by releasing photon/ external capture?), and hence the total E1 ground state contribution is a combination of the cross sections of the nuclear reactions that give rise to a 1^- state. Similarly, all the 2^+ states decay to the ground state, and the total E2 ground state contribution is a combination of the cross sections of the nuclear reactions that give rise to a 2^+ state.

The exact parameters (reduced widths), used to perform the R-matrix fits for each channel, can be found in Appendix Table XXII of (deBoer et al., 2017).

Subthreshold resonance: Broad resonances lurking below the reaction threshold can contribute to the rate as well. This can cause a huge boost over the non-resonant rate.

2 Why is it uncertain? Picked from Giri et al. (2018)

The helium burning stage of red giant stars is dominated by the 3α process and the $12C(\alpha,\gamma)16O$ reaction. A precise understanding of both reactions is necessary because their reaction rates determine the C/O ratio at the end of the helium burning, which is the primary factor to look at for stars undergoing PPSIN, and the BHMG is highly sensitive to this rate. The rate of the 3α process is known with an accuracy of about 12%, but the uncertainty associated with the $12C(\alpha,\gamma)16O$ reaction continues to be an obstacle despite more than four decades of extensive experimental research.

The cross section of the $12C(\alpha,\gamma)16O$ reaction at helium burning energy of $E \approx 300keV$ is dominated by electric dipole $E1$ and electric quadruple $E2$ transitions to the ground state through $J^\pi = 1^-$ and 2^+ sub-threshold resonances and cascade transitions to various sub-threshold states of 16O nucleus. The direct cross section measurement at helium burning energy of 300 keV is impossible in current experimental facilities in the world due to its extremely low cross section of about $\approx 10^{17}$ barn, which is about 5-6 orders of magnitude below the current experimental sensitivity. One way of measuring cross section at low energy is by extrapolating precise high energy data to 300 keV. However, the extrapolation is complicated due to the energy dependence of $E1$ and $E2$ transitions to the ground state, interference effects, and cascade transition contributions. The best way of cross section determination of this reaction at 300 keV is to measure cross sections at the range of high energies and extrapolate them to the helium burning energy of 300 keV by means of R-matrix formalism.

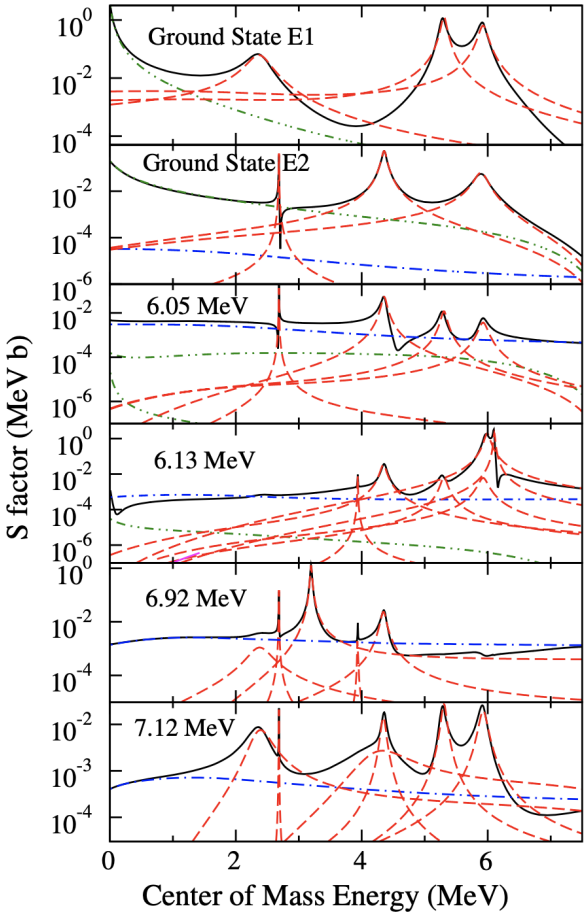

Figure 3: S factors of the different transitions that make up the total $^{12}C(\alpha,\gamma)^{16}O$ cross section. The ground state is further divided into E1 and E2 multipolarities. Dashed red lines indicate individual resonance contributions (single-level calculation), dash-dotted blue lines are the hard-sphere contributions to the external capture, dash-dot-dotted green lines are subthreshold contributions, and the solid black lines represent the total with interferences included (i.e., individual contributions summed coherently).

The final expression for the rate

$$r_{aX} = N_a N_x \langle \sigma(\nu) \rangle$$

with

$$N_A \langle \sigma(\nu) \rangle = N_A \sqrt{\frac{8}{\pi \mu (k_B T)^3}} \int_0^\infty E \sigma(E) exp(-\frac{E}{k_B T}) dE$$

In addition to this, we have the probability of penetration of repulsive potential barrier and the additional S(E) term, which is the astrophysical S factor which contains the same information as $\sigma(E)$ without the strong energy dependence associated with the Coulomb penetration barrier. There are 2 ways to estimate S(E). Either we deal with the domination of non-resonant processes which have a energy-independent S factor. The second case is when the S factor is dominated by narrow isolated resonances. Ignoring all energy dependences except the Lorentzian approximation of the Breit-Wigner cross section, we can get an analytical interpolation. However, the CO reaction is dominated by broad resonances interfering with one another. The product of the Maxwell-Boltzmann and Coulomb parts shows a peak at Gamow peak energy, which is generally much greater than $k_B T$. In some cases, if a nuclear reaction forms a compound nucleus in an excited state, which decays to low energy products. When the energy of an interacting particle matches with one of the energy levels in the range of effective stellar energies, resonances occur and the nuclear reaction rate is often dominated by them. The resonance cross section may be many orders of magnitude greater than that of an off-resonance cross section. Using the selection rules to consider which states are viable to transition from an alpha and carbon nucleus to an excited O nucleus, which decays into a photon, and using parity conservation we can determine some electric and magnetic multipole transitions, the probablity of which is estimated by the Weisskopf formula. Due to isospin symmetry breaking, E1 transitions are suppressed, and E2 make significant more contributions than normal.

In practice, the reaction rate of the $12C(\alpha, \gamma)16O$ is calculated using an R-matrix parameterization and the numerical integration of the above rate equation, and the narrow resonance contributions that are calculated through a Breit-Wigner approximation. This basically uses the approximation that the contributions are negligible outside the narrow range, and using the rectangular approximation for the integral. Narrow resonances are easy to analytically evaluate, whereas broad resonances are a pain because they make extrapolation of the reaction rate at very low energies (via the S factor) a sketchy enterprise. Also, broad resonances below the reaction threshold can contribute to the rate as well, which can cause a huge boost.

REACLIB, which contains thermonuclear reaction rates in parameterized and tabular form Rates are based on published experimentally constrained and otherwise purely theoretical rates. For astrophysics, we see how the abundance changes for each isotope at each step in time based on the production and destruction via all mechanisms and often to include the energy generation from said reactions. These differential equations are very stiff, and sensitive to small changes.

2.1 Uncertinity Analysis

The total uncertainty of the capture cross section, and subsequent reaction rate, resulting from the R -matrix analysis has significant contributions from both the experimental observables and the phenomenological model.
Firstly, ground state E2 data are not always well reproduced by the R-matrix fit and that they show significant discrepancies between one another.
One of the largest sources of uncertainty in an R-matrix analysis can come from different possible

interference solutions that cannot be ruled out by the data. These different solutions are a result of the different possible signs for the reduced-width amplitudes.
For E1 crossection, the ambiguity in the interference sign between the $1^- E_x$ subthreshold state and the E_x unbound state leads to the highest uncertainty. However, there are a vareity of constraints, and there is strong reason to believe that there is only one viable interference solution for both E1 and E2.
For cascade transitions, there is almost no data above a certain threshold.
The reduced χ^2 values for the β-delayed α emission spectra and the scattering data are also significantly greater than 1, likely a result of only approximate modeling of the remaining experimental effects reported in the data. This may even suggest that there are additional unaccounted for uncertainties in the data or, very likely, that the models used to correct for remaining experimental effects in the data are insufficiently accurate.
A long-standing complication with R-matrix theory is that it requires two sets of model parameters: channel radii and background poles, which are correlated to one another, hence there is a range of viable solutions. A phenomenological R-matrix fit must then be tested for its sensitivity to the choice of both the channel radii and poles. The current fit is highly sensitive to the channel radii, however 5.43fm agrees to a high degree. If experimental measurements and uncertainties are taken at face value and model uncertainties are ignored, and the uncertainty in the extrapolation of the R-matrix to low energy is calculated, an uncertainty of only a few percent is obtained.

Another thing to keep in mind is that if we include additional changes to the E2 resonances, and we end up changing the CO rate, there is a correlation between this rate and C burning or O burning, then these additional changes need to be incorporated as well.

3 Comparing the Libraries used

The default library in MESA in REACLIB. This includes multiple databases and when available, NACRE is used as default. Farmer et al, in their 2020 paper, use the STARLIB databse, whereas, the papers we are currently studying use NACRE.

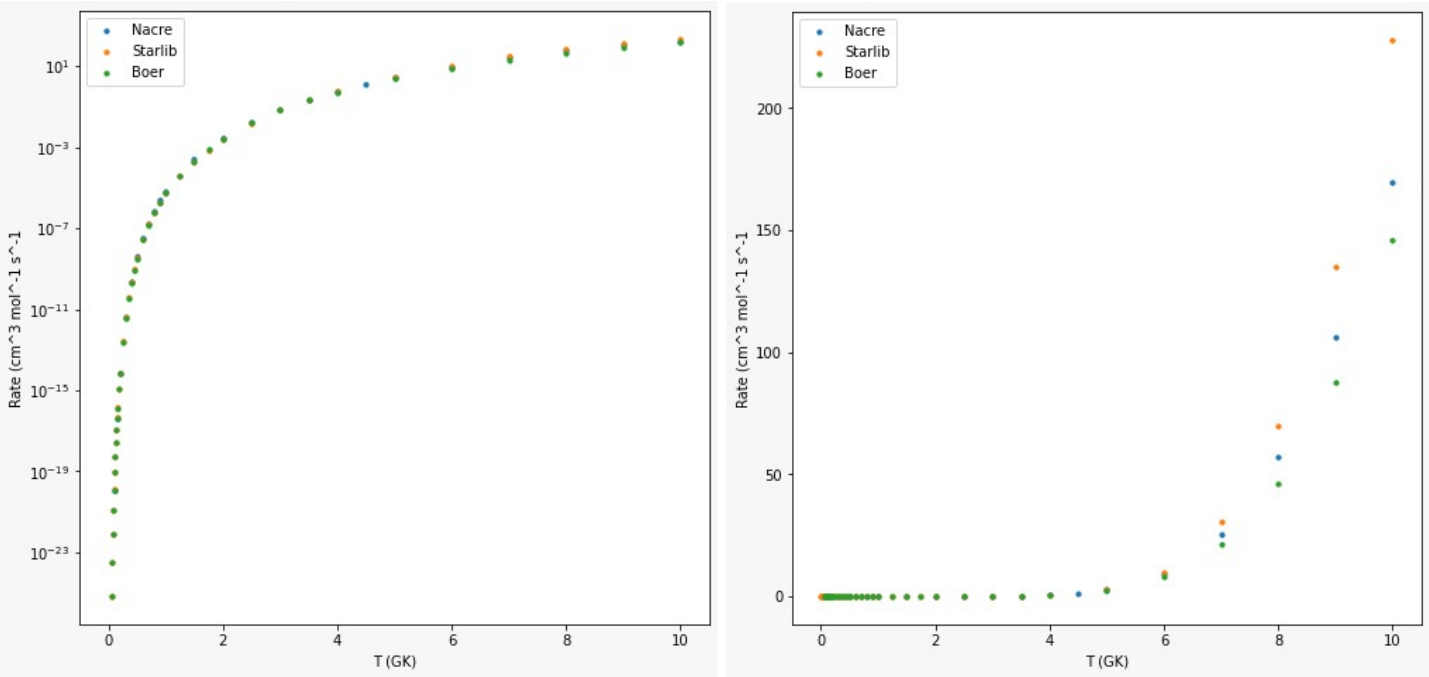

Figure 4: Left: Comparison of reaction rates of NACRE, Starlib, and (deBoer et al., 2017) as a function of 10^9 K on a linear scale. Right: Comparison on a log-scale.

Source	Lower [$M_\odot$]	Upper [$M_\odot$]
1.7× Caughlan & Fowler (1988)	49	135
Angulo et al. (1999) (`NACRE`)	49	130
Kunz et al. (2002)[a]	50	134
Cyburt et al. (2010) (`REACLIB`)	50	136
Sallaska et al. (2013) (`STARLIB`)[b]	47^{+7}_{-2}	130^{+13}_{-7}
deBoer et al. (2017)[c]	51^{+0}_{-4}	134^{+5}_{-5}

[a] Based on the "adopted" fitting coefficents in Table 5 of Kunz et al. (2002)

[b] The `STARLIB` median rate is based on $\sqrt{R_{Low} \times R_{High}}$ (eqaution 17 Sallaska et al. (2013)), where the rates R_{Low} and R_{High} come from Table 5 of Kunz et al. (2002)

[c] Based on the "adopted", "lower", and "upper" rates from Table XXV of deBoer et al. (2017)

Figure 5: Location of the edges of the PISN mass gap for different sources of $12C(\alpha,\gamma)16O$. Uncertainties are 1σ wherever quoted (Farmer et al., 2020)

In addition, (Farmer et al., 2020) also estimate that for assuming that the primary blackhole in GW190521 was a first generation black hole, $\sigma_{C12} = -2.4^{0.6}$ and $S(300keV) = 73^{+11}$ keV barns is needed. I we assume that just the secondary object was a first generation black hole $\sigma_{C12} = -1.7^{+1.8}_{-0.5}$ and $S(300keV) = 87^{+84}_{-12}$ keV barns is needed.

4 Plots from MESA

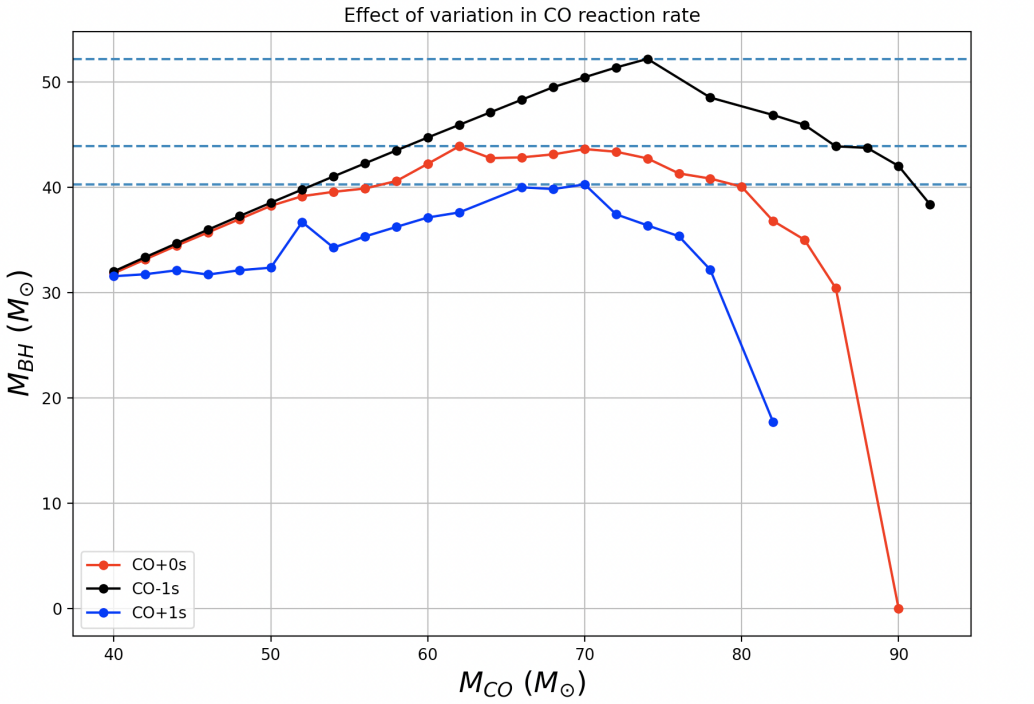

Figure 6: Final BH mass as a function of CO core mass (taken at He depletion) for different CO reaction rates within 1σ uncertainty. Rates were adopted from (Farmer et al., 2020), which use STARLIB

References

R. J. deBoer, J. Gorres, M. Wiescher, R. E. Azuma, A. Best, C. R. Brune, C. E. Fields, S. Jones, M. Pignatari, D. Sayre, K. Smith, F. X. Timmes, and E. Uberseder. The c12(,)o16 reaction and its implications for stellar helium burning. *Reviews of Modern Physics*, 89(3), 9 2017. doi: 10.1103/RevModPhys.89.035007.

P. Descouvemont. Nuclear reactions of astrophysical interest. *Frontiers in Astronomy and Space Sciences*, 7:9, Apr. 2020. doi: 10.3389/fspas.2020.00009.

R. Farmer, M. Renzo, S. E. de Mink, M. Fishbach, and S. Justham. Constraints from Gravitational-wave Detections of Binary Black Hole Mergers on the ^{12}C(α, γ)^{16}O Rate. , 902(2):L36, Oct. 2020. doi: 10.3847/2041-8213/abbadd.

R. Giri, C. R. Brune, S. N. Paneru, D. S. Connolly, B. Davids, D. A. Hutcheon, A. Lennarz, L. Martin, C. Ruiz, U. Greife, U. Hager, G. Christian, and A. Hussein. Cross Section Measurements of the ^{12}C(α , γ)^{16}O Reaction at $E_{c.m.}$ = 3 . 7 , 4 . 0 , and 4 . 2 MeV. In *APS April Meeting Abstracts*, volume 2018 of *APS Meeting Abstracts*, page S11.002, Jan. 2018.